# Temperature Stability of PAG-Doped-Graphene: Towards Commercial Production of Graphene Integrated Circuits

H. Al-Mumen[*,**] and W. Li[*]

[*]Michigan State University, MI, USA, almumenh@msu.edu
[**]University of Babylon, Babylon, Iraq

## ABSTRACT

In this paper we demonstrated the temperature stability of the graphene field effect transistor (FET), which was n-doped by photoacid genrater (PAG), one of the chemical components of the SU-8 photo resist.We studied the current transfer characteristics in a temperature range from ~ -15 $^0$C to + 100 $^0$C and only a small shift in the Dirac point was observed. The temperature dependence of Raman spectra of both pristine and *n*-doped graphene samples were also studied. The experimental results show that the elevating temperature leads to the downward shift of the Raman G-band peak to a lower frequency. The extracted negative temperature coefficients of G-mode for mono- and bi-layer graphene were -0.042 cm$^{-1}$/$^0$C and -0.023 cm$^{-1}$/$^0$C, respectively. Whereas for the SU-8 doped graphene, was -0.0692 cm$^{-1}$/$^0$C and -0.0024 cm$^{-1}$/$^0$C, for mono- and bi-layer graphene respectively. The highest temperature coefficient of the *n*-doped mono-layer can be attributed to the inharmonic coupling of phonon modes and to the effect of the high thermal expansion of SU-8 on graphene.

***Keywords***: graphene, transistor, doping, temperature stability

## 1 INTRODUCTION

Chemical doping has been proven to be an effective solution to open the band gap and modulate the electrical properties of graphene. In this case, the absorption of chemical molecules and/or charge exchange on graphene surface can cause the shift of the initial Fermi level position upward (as shown in *n*-type graphene) or downward (as shown in *p*-type graphene) with respect to the charge neutrality point (the Dirac point). Compared to *p*-type doping, graphene *n*-type doping with long-term chemical stability is more challenging due to the rapid degradation of *n*-type properties upon exposure to air. The degradation of the *n*-type properties is mainly attributed to the absorption of oxygen molecules, which are known as effective hole-dopant for graphene. Electron transfer from the *n*-type graphene to the absorbed oxygen molecules will result in the reduction of the *n*-type doping concentration, which can be well quantified by the electronic band structure and the downward shift in the Fermi level of the doped graphene.

To date, a number of doping approaches have been developed to achieve *n*-type graphene: for example, substitution doping with nitrogen dopants [1-4], covalent functionalization [5, 6], and radiation-induced doping [7, 8]. However, these existing methods usually increase defects in carbon lattices, deteriorate the carrier mobility of as-doped graphene, and are limited in chemical stability.

To mitigate these drawbacks, we proposed, in our previous work [9], a new technique for *n*-type graphene doping with minimum defects and enhanced chemical stability using SU-8 photoresist as a doping and encapsulating material. The fabrication of the *n*-type graphene transistors is fully compatible with microfabrication technology, which provides possibilities for mass production of large-scale graphene-based electronics. In the following section we will investigate the temperature stability of the n-doped graphene FET and then Raman temperature dependent will study for further understanding the effects of temperature variations on doped graphene on crystal structure and phonons.

## 2 METHOD

Pristine graphene (PG) samples were mechanically exfoliated from highly oriented pyrolytic graphite (HOPG) flakes and then transferred onto $SiO_2$ (300 nm)/Si substrates. The graphene samples were then annealed at ~ 400 °C in an $Ar/H_2$ environment for 1 h to remove tape residues and contaminations. The transistors were constructed prior to the SU-8 doping, using the following fabrication method. Briefly, PG samples were patterned into regular shapes via oxygen plasma etching with 150 W RF power, 10 sccm oxygen flow rate, 315 mTorr chamber pressure, and 1 min duration. Ti (5 nm)/Au (70 nm) electrodes were fabricated on top of the graphene as source and drain contacts, via thermal evaporation, electron beam lithography (EBL), and metal lift-off processes. A 140-nm polymethyl methacrylate (PMMA) layer served as a protective layer for the oxygen plasma and a mask for the lift-off. The PMMA resist was dissolved with acetone, rinsed with isopropanol alcohol and de-ionized (DI) water, and then dried with nitrogen. Metal was deposited on the backside of the highly doped Si substrate as the back gate of the transistor. After metallization, graphene nanomeshes (GNMs) with a hole diameter of ~ 100 nm and a neck width

of ~ 300 nm were selectively patterned on the PG at the location of the transistor channel, using an unconventional EBL method [10]. GNM transistors are expected to have relatively higher on/off current ratios compared to PG transistors. This allows for favorably high driving current of the channel compared to the graphene nanoribbon. Furthermore, these nanomeshes can enhance the *p*-type doping level of graphene due to the high sensitivity and reactivity of abundant edge defects.

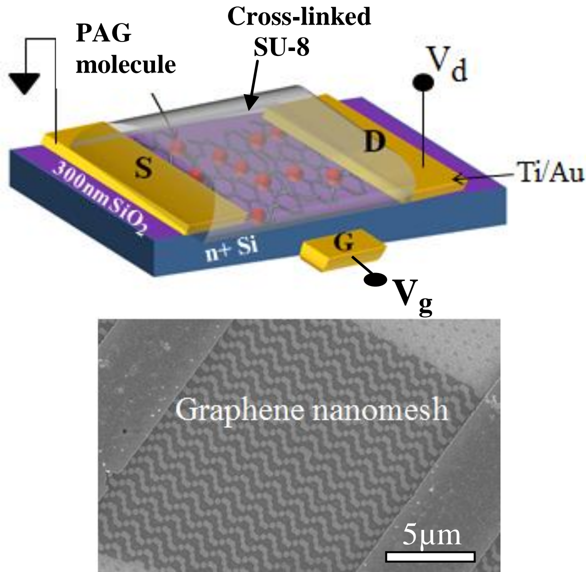


Figure 1: Fabricated n-type graphene nanomesh FET: (a) Schematic of the device. (b) SEM image of the device before doping.

The *n*-type doping of PG or *p*-type GNMs was performed by spinning 4-µm-thick SU-8 2 negative photoresist (NANO™, MicroChem) on the graphene surface. The SU-8 resist contains three basic components an EPON SU-8 epoxy resin, a gamma-butyrolactone (GBL) solvent, and a photo-acid generator taken from the family of the triarylium-sulfonium salts [11]. Following the spin coating, the resist was pre-baked at 95 °C for 3 min to evaporate the GBL solvent and solidify the resist. Optionally, some SU-8-coated samples were exposed to ultraviolet (UV) radiation for 20 sec and then post-baked at 95 °C for 3 min to convert part of the PAG into photo acid to help in SU-8 cross linking, leaving the rest of the PAG to function as a dopant.

## 3 Temperature Stability of the SU-8 Doped Graphene FET

The temperature stability or operation temperature range of graphene transistor is one of the important factors that have to be taken into account. Therefore, we studied the current transfer characteristics of graphene FETs doped with cross-linked SU-8, in a wide temperature range from ~ -15 °C to + 100 °C. Figure 2 demonstrates the temperature stability of the *n*-type properties of two different devices within the testing temperature range, in which only a small shift in the Dirac point was observed. This means that n-doping was consistence at that range of temperature. The increasing in the drain current can be attributed to the negative temperature coefficient behavior of graphene.

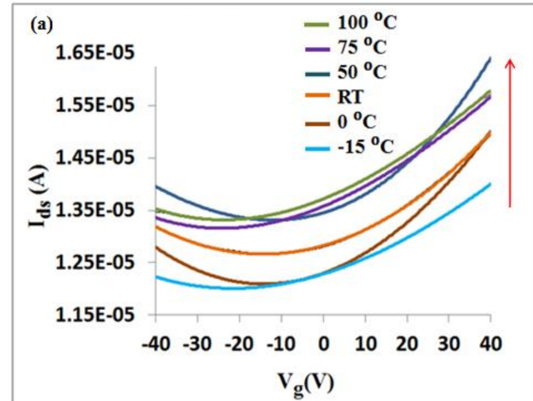


Figure 2: $V_g$-$I_{ds}$ curves at a temperature range from -15 to 100 °C after doping.

## 4 Temperature dependence of Raman Spectra of Graphene FETs

To better understand the temperature effect on SU-8 doped graphene crystalline structure, such as atomic bonds, phonons, and thermal expansion, we studied the temperature dependence of Raman spectra of both pristine and *n*-doped graphene samples. During the measurements, the samples were placed on a hot stage under a HoloProb Raman spectroscope. All the spectra were excited using a visible (532 nm) laser with a relatively low laser power (0.53 mW) to avoid graphene heating by the excitation laser. A 100× objective lens was used to focus the laser beam on the desired location of the sample. The temperature dependence of the G-band peak position was measured at several temperatures varying from room temperature (RT) to 150 °C for both the *n*-doped and pristine graphene FETs.

First, the temperature dependence of pristine mono- and bilayer graphene was investigated. The experimental results show that the elevating temperature leads to the downward shift of the Raman G-band peak to a lower frequency (Figure 3). The extracted negative temperature coefficients of G-mode for mono- and bi-layer graphene were -0.042 $cm^{-1}$/°C and -0.023 $cm^{-1}$/°C, respectively.

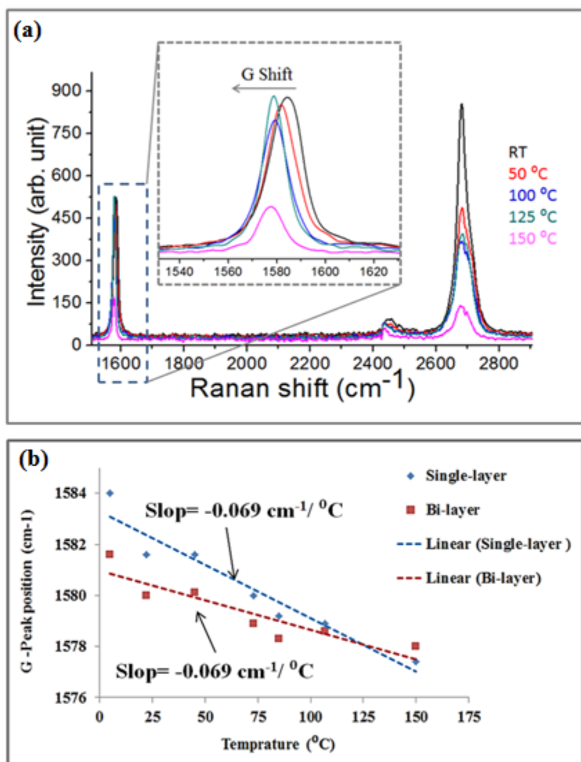


Figure 3 (a) Raman spectra of pristine graphene at different temperatures. (b) Temperature dependence of G-band peak for mono- and bilayer pristine graphene samples.

Second, the temperature dependence of SU-8 doped *n*-type graphene FET was investigated, as given in Figure 4 Another peak appeared at 1607 $cm^{-1}$, which was the characteristic peak of the SU-8 resist. One remarkable observation is that the G-band peak of the *n*-type graphene became wider as the temperature elevated. The corresponded G-mode temperature coefficients of *n*-doped mono- and bilayer were determined to be -0.0692 and -0.0024 $cm^{-1}$/ºC, respectively (Figure 4 (b) and (c)). The results indicate that the G-mode temperature coefficient of the *n*-doped monolayer graphene had a highest sensitivity to temperature.

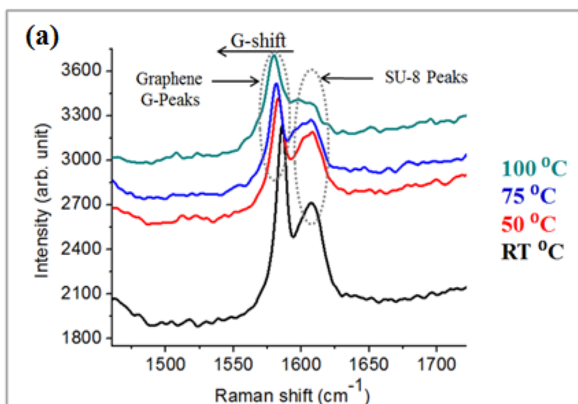


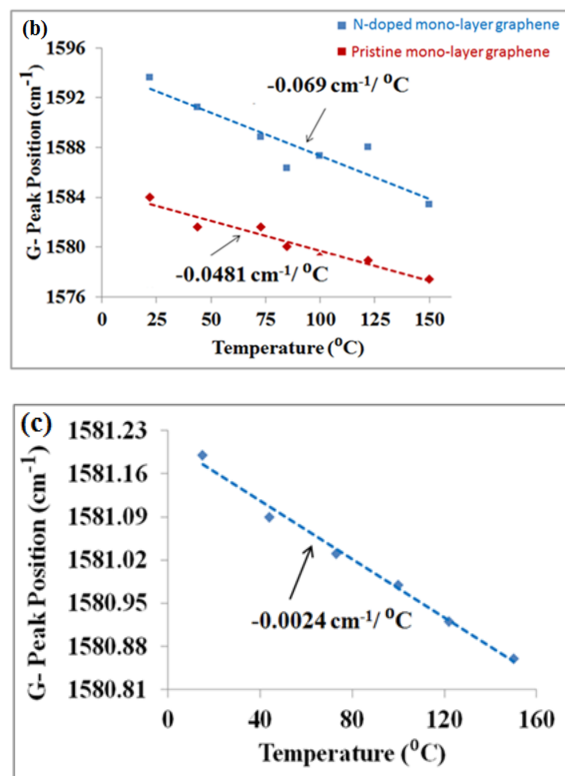


Figure 4 (a) Raman spectra of n-doped graphene at different temperatures. (b) Comparison of temperature dependence between pristine and n-doped monolayer graphene sheets. (c) Temperature dependence of bilayer graphene. The slope of fitting curve represents the extracted temperature coefficient of G-band peak.

The mechanism of the temperature-dependent downshift of the G-band peak are the elongation of the C-C bonds due to high thermal expansion effect of the SU-8 or non harmonic coupling of phonon modes [12]. The temperature dependence of the G-band can be represented by $\omega = \omega_0 + XT$, where $\omega$ is the frequency of the G-mode, $X$ is the first-order temperature coefficient defined by the slope of the temperature dependent curve, $T$ is the initial temperature value, and $\omega_0$ is the G shift at the initial temperature. The measured frequency change $\Delta\omega = \omega - \omega_0$ can be written as [13]: $\Delta\omega = (X_T + X_V)\Delta T = (\partial\omega/\partial T)\Delta T + (\partial\omega/\partial V)\Delta V$, where $X_T$ and $X_V$ are the frequency shifts due to the intrinsic temperature effect as well as the thermal expansion that induces volume change. The similar effect was also reported in [14], where the G-band peak of suspended graphene shifted to a lower value as a tension force was applied to its surface. Therefore, the G-band shift can be used as an indicator not only for the thermal impact but also for mechanical impact on graphene.

It is of note that the $Si/SiO_2$ substrate does not strongly affect the thermal coefficient ($X$) since the measured G-band at ~ 1582 $cm^{-1}$ is made up of the optical phonons due to the in-plane vibrations. In addition, the $E_{2g}$ symmetry of

the G-band confines the motion of the atoms to the plane of the carbon atoms [15]. The out-of-plane vibrations (ZO phonons) in graphene are not coupled to the in-plane motion that defines the G-band spectrum position. The out-of-plane vibrations are expected to be more associated with the substrate influence [16]. Therefore, the G-band temperature dependence is mostly the properties of the graphene layer rather than the substrate characteristic. Furthermore, the thermal expansion coefficient for $SiO_2$ is low ($2.6\times10^{-6}$) $C^{-1}$, which does not induce thermal stress to the graphene layer.

## 3 CONCLUSION

The n-type effect of the as-doped devices was demonstrated to be chemically stable in air. Additionally, the *n*-doped graphene FET was stable between - 22 °C and 100 °C with no significant shifting in the Dirac point. The temperature effect on the doped and pristine graphene crystalline structure was also studied. The G-mode of the doped monolayer graphene was demonstrated to have a greater sensitivity to temperature in comparison to the pristine graphene, whereas the doped bilayer graphene showed a relatively lower sensitivity. The left shifting of the G-mode with elevated temperature indicates that an expansion occurred in graphene sheet.

## REFERENCE


[1] H. Al-Mumen, F. Rao, L. Dong, and W. Li, in *The 8th Annual IEEE International Conference on Nano/Micro Engineered and Molecular Systems (IEEE NEMS 2013)*, Suzhou, China, 2013.

[2] F. Ru and J. F. Richard, *Journal of Micromechanics and Microengineering,* vol. 13, pp. 80, 2003.

[3] K. Stephan, B. Gabriela, L. Michael, H. Daniel, and B. Anja, *Journal of Micromechanics and Microengineering,* vol. 18, pp. 125020, 2008.

[4] Y. Wang, M. Bachman, C. E. Sims, G. P. Li, and N. L. Allbritton, *Langmuir,* vol. 22, pp. 2719-2725, 2013/07/09 2006.

[5] D. Graf, F. Molitor, K. Ensslin, C. Stampfer, A. Jungen, C. Hierold, and L. Wirtz, *Nano Letters,* vol. 7, pp. 238-242, 2007.

[6] Y. C. Lin, C. Y. Lin, and P. W. Chiu, *Applied Physics Letters,* vol. 96, 133110, 2010.

[7] C. H. Zhang, L. Fu, N. Liu, M. H. Liu, Y. Y. Wang, and Z. F. Liu, *Advanced Materials,* vol. 23, pp. 1020-1024, 2011.

[8] T. C. Li and S.-P. Lu, *Physical Review B,* vol. 77, 085408, 2008.

[9] H. Al-Mumen, L. Dong and W. Li, applied Physics Letters, vol 103, 232113, 2013.

[10] F. Sols, F. Guinea, and A. H. C. Neto, *Physical Review Letters,* vol. 99, 166803, 2007.

[11] Z. Chen, I. Santoso, R. Wang, L. F. Xie, H. Y. Mao, H. Huang, Y. Z. Wang, X. Y. Gao, Z. K. Chen, D. Ma, A. T. S. Wee, and W. Chen, *Applied Physics Letters,* vol. 96, 213104, 2010.

[12] L. Ci, Z. Zhou, L. Song, X. Yan, D. Liu, H. Yuan, Y. Gao, J. Wang, L. Liu, and W. Zhou, *Applied physics letters,* vol. 82, pp. 3098-3100, 2003.

[13] I. Calizo, A. Balandin, W. Bao, F. Miao, and C. Lau, *Nano Letters,* vol. 7, pp. 2645-2649, 2007.

[14] G. Tsoukleri, J. Parthenios, K. Papagelis, R. Jalil, A. C. Ferrari, A. K. Geim, K. S. Novoselov, and C. Galiotis, *Small,* vol. 5, pp. 2397-2402, 2009.

[15] F. Tuinstra and J. L. Koenig, *The Journal of Chemical Physics,* vol. 53,1126, 1970.

[16] N. Mounet and N. Marzari, *arXiv preprint cond-mat/0412643,* 2004.